SSRG International Journal of Civil Engineering
ISSN: 2348-8352/ https://doi.org/10.14445/23488352/IJCE-V13I9P119

Volume 13 Issue 9, 320-338, September 2026

Original Article

Effects of Multiple Precursors on Bond Strength and Flexural Performance of Ambiently Cured on Geopolymer Concrete

Baskara Sundararaj J[1], Kannan Rajkumar P R[2]

[1]Centre for Advanced Concrete Research, Department of Civil Engineering, SRM Institute of Science and Technology, Kattankulathur, Tamil Nadu, India.
[2]Department of Civil Engineering, SRM Institute of Science and Technology, Kattankulathur, Tamil Nadu, India.

[1]Corresponding Author : baskaraj@srmist.edu.in

Received: 27 March 2026 Revised: 08 September 2026 Accepted: 11 September 2026 Published: 29 September 2026

Abstract *- The present study investigates the bond strength and flexural behavior Of Geopolymer-based Reinforced Concrete (GPRC) beams to assess their suitability as sustainable alternatives to conventional concrete structures. Geopolymer Concrete (GPC) prepared with industrial byproducts, Fly Ash (FA), Ground Granulated Blast Furnace Slag (GGBS), and Silica Fume (SF), is environmentally friendly due to its significantly reduced carbon footprint. Tests involved an extensive set of experiments on GPRC beams to determine mechanical properties, steel–GPC interface BS, and flexural behavior. Experimental results are analyzed here using critical structural performance parameters such as crack initiation-propagation, failure modes, ultimate load-carrying capacity, moment versus deflection, strain response, end rotations and ductility ratios. For mixes GP30M4, GP50M4, and GP70M4 with hidden reinforcement, 12-mm-diameter rebars replaced by 10-mm-diameter rebars indicated an improvement in BS of 3.82%, 5.61%, and 6.51%, respectively. Similarly, in the case of 10-mm-diameter reinforcement, the BS for mix GP70M4 exhibited up to a 69.12% increase compared to mix GP30M4. Similarly, the ultimate load-carrying capacity of GP70M4 beams showed an 8.79% increase compared to GP30M4 beams. A higher initial deflection was observed in GP30M4 beams because of the diminished modulus of elasticity, reflecting the aspect of crack control; however, these features are favorable in the case of higher-grade concrete. In conclusion, GP70M4 GPRC provided BS comparable to or even superior to that of GP30M4 GPRC, while tests related to flexure showed improved capacity and ductility. Outcomes confirm the structural efficiency of GPC concrete and recommend its application as an environmentally green option.*

Keywords *- Geopolymer Reinforced Concrete, Geopolymer Concrete, Bond Strength, Crack patterns, Ultimate load capacity, Midspan displacement, Strain behavior, End rotation and Ductility ratio.*

1. Introduction

GPC is an innovative and eco-friendly cementitious material that utilizes industrial by-products such as FA and GGBS as binding agents in place of traditional Ordinary Portland Cement (OPC) [1]. This environmentally friendly material reduces the carbon dioxide emissions during its entire production process and develops mechanical properties that are comparable with those of Conventional Concretes (CC), making it available in modern concreting works [2]. GPC comprise fine and coarse aggregates, admixtures, aluminosilicate co-products like FA and GGBS, which are activated by alkali-based solutions. It is desired to reduce the carbon footprint in concreting, particularly in low-hazardous applications like pavements and footpaths [3, 4]. Comparing OPC with GPC based on CO_2 emissions really shows the great ecological advantages that GPC possesses [5]. Studies have deduced that these concretes can achieve reduces CO_2 emissions by up to 80% relative to conventional OPC, mainly because of the exploitation pertaining to industrial co-products, which require less energy during their production [6, 7]. In this respect, the energy input to develop GPC is considerably lower than that consumed for OPC concretes, approximately 0.110 kWh/g, hence with better sustainability [8].

The focus on GGBS and ceramic dust. It analyzes the properties of GPC with GGBS replacement, revealing enhanced compressive strength and superior chloride ion resistance [9]. The influence of micro silica on the performance of high-strength GPC made from GGBS at high volumes was investigated. The investigation considered parameters like water absorption capacity, workability, splitting tensile strength, and compressive strength. Cluster investigations were done by considering the compressive strength and water absorption capacity to reveal the relationship between all those mentioned parameters. Investigation of the correlation between split tensile strength, water absorption capacity, and compressive strength was also done [10].

The Bond Strength (BS) in GPC is found to be significantly higher than in OPC, with a mean BS of 14.3 MPa in Metakaolin (MK) calcium carbide residue-based GPC, which is above a 105% increase over OPC bond strength [11]. Studies have established a relationship between BS and Compressive Strength (CS), with a FA-based GPC showing an augmentation in BS of 1.97 to 2.56 times as the CS increased proportionally from 20.33 MPa to 41.12 MPa [12]. The bond properties of GPC in combination with reinforcing bars, such as steel and ribbed Glass Fiber Reinforced Polymers (RGFRC), illustrate equal bond strengths and stress-slip resistance. The study highlights the pronounced influence of factors such as rebar diameter, bond length, and surface treatment on bond effectiveness [13].

GPC shows higher BS properties in contrast to those of OPC due to higher CS and dense microstructure. A study on bond slip mechanics of GPC with Carbon Fiber-Reinforced Polymer (CFRP) and Investigations into GFRP bars have been undertaken to demonstrate their effective bond strength transfer methods and failure modes [14]. BS properties of GPC have proved better compared to those of OPC concrete. Increased embed length and bar diameter were found to reduce BS in both GPC and ordinary OPC concrete, but slip increased simultaneously [15]. The BS of GPC can be controlled in terms of CS and the length of embedment of reinforcing bar. Higher CS promotes higher BS, but increased embedment length decreases BS based on experimental studies [16].

Studies have proven that Geopolymer Concrete Beams (GPCB) have equal bending qualities to OPC beams with respect to cracking behaviour, failure patterns, and load versus deflection behaviour [17, 18]. This study examines the bending properties for twelve BFRP reinforced concrete beam samples (size 180 × 300 × 2200mm), consisting of eight GPCB samples and four Ordinary Portland Cement (OPC) beam samples, subjected to high temperatures. The beam samples were subjected to higher temperatures at values of 200°C, 400°C, and 600 °C. The findings indicate that the mechanical properties were sustained for temperatures below 400°C for GPC, while beyond this value, the properties degraded significantly. Finally, it is concluded that the GPC beam reinforced with BFRP possessed higher stiffness values as well as resistance against cracks compared to their OPC counterparts [19].

The bending qualities of GPC have proved to be better than those of OPC concrete, based on this analysis. From the FEM analysis, GPCBs have proved to have a better post-yield stiffness with a 44% increment and a 12% increment in ductility over OPC beams, despite the higher CS of GPC. Generally, this implies that GPC not only shows better performance in bending but is also more resilient to damage in structures, making it a preferable substitute for CC materials [20]. The bending performance of GPCBs shows analogous behaviour to CC beams. The GPCBs show a 7.4% enhancement in the load-carrying capacity of bending moments, a 60% reduction in stiffness, a 28% reduction in ductility, and a 18.3% increment in toughness over CC beams. Increased depth is beneficial in improving ductility, but a higher reinforcement ratio leads to a reduction in ductility. The analysis shows that using the Egyptian professional standards ECP 203 or ACI 318 can be safe in designing under-reinforced GPC flexural beam components [21].

The analysis showed that One-Part GRCBs have equal flexural performance capabilities compared to conventional OPC concrete beams. The two possessed equal cracking patterns, failure modes, load versus deflection behaviour, and strain profiles. The investigation used four-point loading tests performed on nine specimens, which indicated that one-part GRCBs were able to retain a considerable amount of their strengths under flexural loads, thus validating them as a potential substitute for CC in construction work [17]. The manuscript highlights the flexural performance capabilities of GPC-beams reinforced with different substances such as FA, GGBS, and MK. The mixture F50G25M25 demonstrated a notable enhancement in Flexural Strength (FS) was observed in comparison to the control specimen [22]. The manuscript studies GGBS-Dolomite GPC specimens under cyclic loading, which were compared with another specimen made of OPC, focusing on the role of steel fibers with an optimum mix of 70:30 of GGBS and Dolomite to maximize the resulting CS [23].

The study focuses on GPRC beams using Incinerated Bio-Medical Waste Ash and GGBS. The study analyses the flexural performance with varying quantities of Waste Glass Powder (WGP) used as a fine aggregate [24]. The manuscript focuses on fly-ash GPCBs reinforced with CFRP and GFRP bars instead of studying various binding materials. The manuscript analyses the flexural performance, ultimate load-carrying capacity, and failure modes, explaining the influence of varying reinforcement proportions and types in detail [25]. The manuscript focuses on hybrid fiber-reinforced ternary mix GPCBs incorporating crimped steel and Polypropylene fibers rather than other binding materials. The manuscript highlights the flexural performance analysis of these beams under monotonic loading situations [26].

The flexibility analysis of GPCBs, studied in this analysis, shows a high load-displacement behaviour and a FS equal to conventional Portland cement beams. The study highlights how this performance can be affected by both the longitudinal reinforcement ratio and the shear span-to-depth factor. Finite element nonlinear analysis, developed according to the properties present in GPC, successfully predicted the strength and deflection, demonstrating the possibility of using sustainable self-compacting GPC in this field [27]. A cyclic load was used in assessing the flexural performance of GPCBs, focusing on load-deflection behaviour, initial cracking load, ultimate load, ductility index, and cracking mode. The results demonstrated a higher ductility index, which ranged from an 11% to 44% increase, when using steel fibers (between 0.25% and 0.75% volume fraction). Additionally, it has been observed that GPC has a cost/ultimate load ratio 16% better in GPC compared to cement concrete, making GPCBs not only better in performance but more economical too [28].

Through empirical testing, the flexural performance of alkali-activated ultra-high-performance GRCBs was assessed under four-point bending conditions with a high level of strictness. It can be said that the flexural capacity and rigidity of the beams were increased with respect to a higher percentage of steel fibers. It was observed that the augmentation of the reinforcement ratio from 1.18% to 2.32% improved flexural capacity by about 60.5%, with an improvement of 12.3% in flexural stiffness, while higher fractions of steel fibers enhanced the flexural capacity and stiffness by about 4.7% and 4.4%, respectively [29].

Engineered Geopolymer (GP) Composite (EGC), known for its environmental viability, was adopted to study the flexural performance of the EGC-concrete was investigated. The designed beams containing three varied EGC dimensions of 20, 40, and 60mm, inclusive of two surface treatments, scabbling and grooving, along with varied casting sequences, were put to test at four-point bending. Detailed parametric analysis was also executed. Failure modality, energy efficiency, ductility, and mechanisms for controlling crack widths were considered [30].

The application of GPC combined with steel connectors resulted in significant enhancement regarding flexural performance. The increments of connectors placed near supports increased the first crack load by 6.67% to 42.22%, the service load by 16.22% to 36.20%, and the load-carrying capacity by 12.00% to 24.80%. The shift in the failure mechanism from traditional tensile failure to the phenomenon of concrete fragmentation shows the effectiveness of using a steel composite reinforcement in the beam [31].

In the research, the flexural performance of GPCBs is observed to be comparable to that of structural grade M30 Reinforced Concrete Beams (RCBs). The investigation results are regarded as having strong split tensile strength, stiffness characteristics, and energy capacity with appreciable ductility. Further, the deflection and stiffness degradation at critical stages was also seen to be comparable, and thus the GPCBs can act as a credible substitute for traditional RCBs in flexural applications [32].

2. Research Significance

This paper provides a comprehensive evaluation of reinforced concrete's structural performance that includes GPCs, aimed at evaluating their viability as an eco-friendly substitute for CC. GPC, which is made from industrial by-products like FA, GGBS, and silica fume (SF), is better for the environment because it uses less CC and produces less CO2 emissions than cement does. Even though more people are interested in GP materials, not many thorough studies have been done to look at how GPCs and reinforcing steel bond and the flexural performance of structural members containing these concretes.

The experimental setup includes pouring concrete beams with 10 and 12 mm steel bars in them. The results indicated that the BS of GP70M4 mix was better compared to GP30M4, especially when considering smaller diameter reinforcements. However, the GP30M4 GPC with a reduced elastic modulus showed an increased deflection in the initial phases of loading, thus affecting Crack Resistant Properties.

The load-carrying capacity in all categories of GPCs showed equal capability in carrying maximum load. Additionally, ductility and capacity to withstand energy in GPC can be considered advantageous, thus suitable for application in a ductile structure.

To address these identified deficiencies, the current study concentrates on the assessment of BS and flexural properties of RC beams constructed with GPC by taking into account the variety of influencing parameters such as precursor type and composition, alkali activator concentration, liquid-to-binder ratio, and curing environment.

This article summarizes recent experimental results providing practical recommendations for optimization of GP formulations, whereas earlier reviews typically concentrate on one or two parameters.

Furthermore, well-established mitigation techniques are integrated, new BS and slip behaviour, including crack pattern and its propagation, modes of failure, ultimate capacity in load, moment versus midspan displacement curves, loading point displacement curves, strain behaviour, end rotation) and ductility ratio were carefully measured and compared with observations from all three mixes of GPC specimens. Moreover, the microstructure of the mixture was studied in order to explain some of the performance characteristics of the material.

Thus, the scanning electron microscope analysis, along with energy-dispersive microanalysis (SEM-EDAX) and X-ray diffraction (XRD) analysis were conducted. The microstructure of the modified mixtures was analyzed, and the resulting microstructural characteristics were correlated with the strength properties.

3. Materials and Design of Mixes

3.1. Aluminosilicate Source Materials

3.1.1. Fly Ash

As regards the large-scale analysis, the Class F FA was used. It met all the criteria outlined in ASTM C618-22 [33]. The detailed chemical composition of this material was determined with high precision using X-ray Fluorescence (XRF). XRF analysis was employed to determine the exact chemical composition of each of the precursors (FA, GGBS, and SF). The data collected can be further represented in Table 1 and Figure 1. Furthermore, the discussion about the unique features of FA, GGBS, and SF has been described, and the relevant SEM images of the materials have been provided in Figure 1 for visual interpretation purposes.

3.1.2. GGBS

The GGBS used in the current study has been provided by JSW Cement (Hyderabad, India) and follows the specifications mentioned in ASTM C989-C989M-18a [34].

3.1.3. Silica Fume

The silica fume used in the present study was supplied by Elkem Pvt. Ltd. (Mumbai, India) and complied with the specifications of ASTM C1240-20 [35].

3.2. Aggregates

The fine and coarse aggregates used in this study were particularly engineer-made manufactured sand and crushed granite aggregates. The fine aggregate conformed to Zone II specifications as per IS 383:2016 [36]. Table 2 below shows a detailed physical requirement of aggregates used, with the size distribution curve of M-sand and crushed granite aggregates shown in Figure 2.

3.3. Alkali Activator Solutions

The alkaline activator mixture used to trigger geopolymerization reactions in this research work was a combination of sodium silicate solution (Na_2SiO_3), sodium hydroxide (NaOH lye), and water.

The Na_2SiO_3 used in this research work, which was a commercial water glass solution, had a silica modulus of 2.0 with a chemical composition containing 31.0% SiO_2 and 15.5% Na_2O. NaOH lye with a concentration of 49%, which is approximately 18.7 M, had a higher alkaline concentration necessary for activating aluminosilicate reactants and thus used in this work to create such an alkaline activating environment.

For activating a FA and GGBS, an Alkaline Activating Solution (AAS) was mixed from NaOH lye, Na_2SiO_3 solution, and water in fixed quantities under rigorous proportions.

Two mix proportions of NaOH lye (3.5 M and 5 M) and Na_2SiO_3 solution were used in this research work, namely 1:0.25 and 1:0.67 proportions, thus controlling silica proportions or geopolymerization reactions, resulting in governing mechanical and durability strengths of GPC.

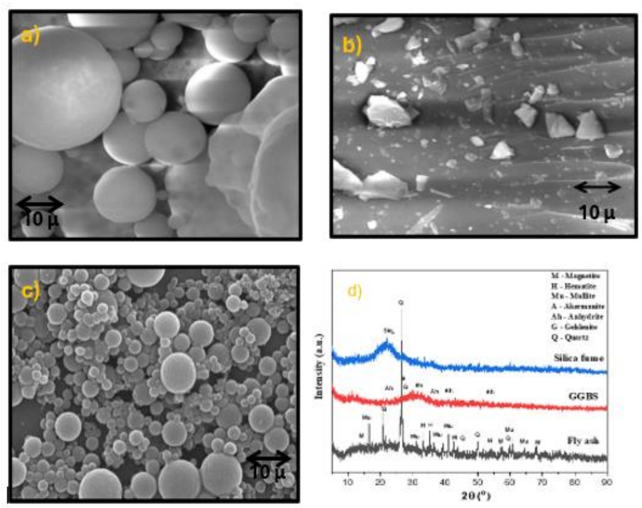

Fig. 1 SEM images and XRD diffractograms of FA, GGBS, and SF

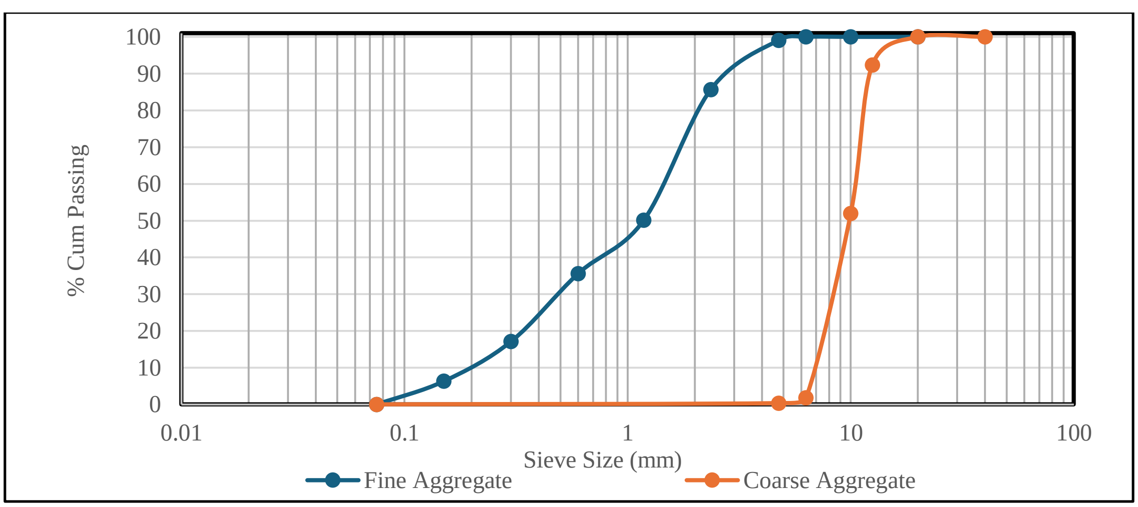

Fig. 2 Aggregates grain-size distributions

Table 1. XRF analysis of the precursor materials (FA, GGBS, and SF)

Composition (%)	SiO_2	Al_2O_3	Fe_2O_3	CaO	MgO	Na_2O	LOI
FA	55	26	10.17	2.09	0.80	0.40	1.30
GGBS	21.58	14.88	1.78	55.25	2.63	0.015	1.175
SF	96.2	0.09	0.63	0.23	0.37	0.09	1.15

Table 2. M. sand and coarse aggregate Properties

Mechanical or Physical attributes	M. Sand	Coarse aggregate
Maximum size (mm)	4.75	12.5
Water absorption (%)	2.75	0.4
Specific gravity	2.72	2.85
Impact value (%)	-	4.36
Crushing value (%)	-	7.54
Sieve analysis	3.1	2.53

3.4. Mix proportions for GPC

One of the main features of GPC mixtures is that their design intrinsically differs from that of CC due to the nature of its binder system. Unlike conventional Portland cement concrete, GPC is based mainly on silica-and-alumina rich precursor materials, such as FA, GGBS, and SF. The precursor materials are involved in a chemical reaction with an alkaline activator solution, resulting in geopolymeric bond formation. These types of bonds effectively bond the aggregates, GP paste, and partially unreacted particles, and hence result in a dense and homogeneous GPC matrix. The exact quantification of the required quantities of FA, GGBS, SF, Na_2SiO_3 solution, and NaOH lye is very crucial in achieving the expected performance of the GP mix. The proportions of these constituents were accurately calculated considering numerous influencing factors, especially the alkaline liquid-to-binder ratio, which controls the reaction kinetics and strength gain in GPC. Table 3 displays the mix proportions that were determined for different GPC classes. Extensive laboratory testing was used to systematically create GP blends. The goal of these experiments was to enhance GPC-workability's fresh and hardened qualities, strength, and durability, both for the improvement of the structural effectiveness and reliability of GPC [37].

3.5. Curing

The specimens were kept under ambient temperature until the hardening of the samples took place. They were demoulded after 24 hours. Demolding time was based on the extent of reactions taking place inside the mixes. Post demolding, the flexural properties associated with the strength of the beam were assessed at 28 days.

Table 3. Presents the mix proportions of the GPC

Mix Id	FA	GGBS	SF	AAS		M-Sand (kg/m^3)	CA kg/m^3	AL/B	Molarity (M)
				NaOH kg/m^3	Na_2SiO_3 (kg/m^3)				
GP30M4	0.7	0.3	0	172.8	43.2	774.1	991.3	0.6	3.5
GP50M4	0.7	0.3	0	129.72	86.48	739.5	947.1	0.47	5
GP70M4	0.65	0.3	0.05	135.24	90.16	739.5	947.1	0.49	5

4. Experimental Investigation

4.1. Bond Strength

To evaluate the anchorage capacity between reinforcing steel and GPC, pull-out tests were conducted according to RILEM recommendations [38–40]. Pull-out test specimens were prepared using cube molds with a cross-sectional dimension of 100 x 100 x 100 mm. To prevent premature splitting failure of concrete during the loading procedure, several specimens were internally reinforced with hidden spiral reinforcement of 6 mm diameter, while other specimens without hidden reinforcement were also made for comparison. The specimens were prepared in such a way that the reinforcing bar was oriented perpendicular to the concrete surface, as shown in Figure 3(a). In each cube sample, the reinforcement was embedded at the center, extending 10 mm beyond the bottom surface. A dial gauge was attached at that point to measure the slip of the rebar from the surrounding concrete with high accuracy during the test. Bond characteristics of the GPC mixes were interpreted using the obtained load–slip response.

The bond stress for the GPC mixes was determined using the mathematical expression described by Equation (1).

$$\text{Bond stress } \tau = \frac{P}{\pi d_r le} \quad (1)$$

Where: P- pull-out load, d_r- diameter of the rebar, le- embedded length of the rebar.

In order to examine the bond behaviour, the pull-out test was done according to IS 2770 (Part I)-2001 [41], as shown in Figure 3(b-c). The tested a total of 12 pull-out samples for each mix, using two different rebars.

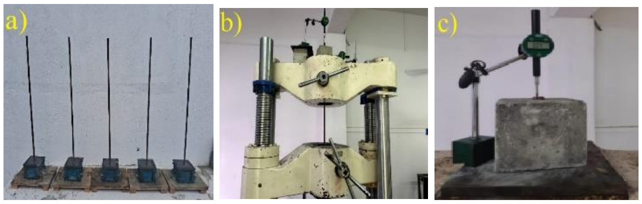

Fig. 3 (a) Bond strength specimen after casting (b) Bond strength Test Setup of GPC, and (c) Measurement of slip value using dial gauge.

4.2. Design and specifications of Flexural Beams

Table 4 shows the specifics of the beams. Three beams were made using GP30M4, GP50M4, and GP70M4. The GP30M4, GP50M4, and GP70M4 beams were particularly designed to be single reinforced beams (SRBs). The effective depth (d) and beam width (b) were kept the same for all of the samples: 150 mm and 191 mm, respectively. To make sure that beams will fail in flexure according to IS 456:2000 [42] recommendations for FS testing, the beam ratio (span/effective depth) was set at 15.7, and the beam length was set at 3000 mm. To ensure adequate support for the flexural beam, it was configured with two 12 mm diameter bars in the tension zone and two 10 mm diameter bars in the compression zone. On this basis, the flexural beam was intentionally designed as a robust structural component. Thus, as seen in Figure 4, two-legged stirrups measuring 8 mm in diameter and 150 mm from center to center were used.

4.3. Sample Preparation and Instrumentation

In accordance with the designed beam, the moulds were prepared using plywood materials. The beam specimen was provided with a sufficient thickness of the GPC protective layer by using a 25 mm cover block. When the longitudinal tensile reinforcement gave way, the specimen was made to create a shear force, which ensured that the beam failed in bending at its midpoint. At the middle of the tension bar's span, a strain gauge was bonded using adhesive. In addition, another strain gauge was fixed at the second stirrup from both ends of the beam. The surfaces of the bars were ground and polished using fine sandpaper prior to fixing the strain gauge.

The GPC was batched and mixed using the specified mix proportions with intensity. The GPC was mixed on a platform that didn't let water through, and then it was poured into the beam mold. Initially, the cementitious components were combined with the measured coarse aggregate and M-sand. Finally, the AAS was added and mixed thoroughly. The slump value of the GPC was checked before it was fed into the mould. The moulds were cleaned and lubricated sufficiently, which could facilitate easy demoulding after casting. Before feeding the GPC into the mould, the reinforcement cages were placed within the mould. After 24 hours of moist curing, the specimen was taken out of the mold and left to cure for another 28 days in normal conditions. Table 5 gives a full description of the beams that were made for the flexural test.

4.4. Test of Flexure Beam

The beam specimen received a treatment of whitewashing, in which the exact sites for mounting the strain gauge, meant for measurement of compression strain, location of the neutral axis, and center lines, were labelled before conducting experiments. The strain gauge was put halfway up on the top of the specimen and in the middle of the front face, with a distance of d/2. The lead wires from the strain gauge were connected to a data gathering system and a 32-channel strain bridge using the full-bridge approach.

Table 4. Details of flexure beams (overall size 3000 X 150 X 230 mm)

Beam identification	Number of tension reinforcement & diameter (mm)	Numbers of compression reinforcement & diameter (mm)	Area of tensile reinforcement, Ast (mm^2)	Percentage of steel reinforcement ρ = Ast/bd (%)
GP30M4	2Y12	2Y10	226.18	0.79
GP50M4				
GP70M4				

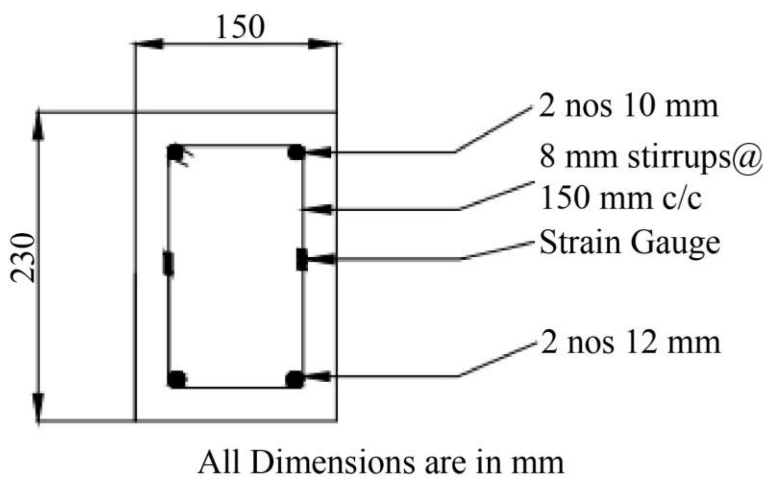

Fig. 4 Diagram of GPC reinforcement

Table 5. Fresh and harden properties of GPC

Parameters	GP30M4	GP50M4	GP70M4
Minimum targeted strength (MPa)	30	50	70
Liquid – binder ratio	0.54	0.42	0.44
Mix ratio	1:2.16:2.75:0.54	1:1.61:2.06:0.42	1:1.61:2.06:0.44
Slump in (mm)	87	70	62
Wet density	2425	2457	2453
28 days harden density	2373	2401	2409
28 days CS (MPa)	40.50	57.24	78.57
28 days FS (MPa)	4.64	5.47	7.46
28 days Split tensile strength (MPa)	3.36	4.63	5.48
Elastic Modulus (GPa)	16.38	24.71	36.42

To measure deflections, the Linear Variable Displacement Transducer (LVDT) sensor was positioned L/3 from the end support, at the load application point, and in the center of the span.

Figures 5 (a) and (b) shows a diagram of the beam specimen was set up for flexural loading tests. To enable efficient working of a data acquisition system, with a view to check soundness of devices, a relieving load had to be applied, followed by an unload stage.

To avoid damage to human life, apparatus, and other devices, a brief loading of the specimen had to be carried out with a load of 0.5, 1, and 5 kN. The specimens were fixed for tests in a simply supported setup with an effective span length of 2.8 m for carrying out tests related to flexural loading. The specimen loading had a four-point loading system.

The specimen tests were conducted under a 100-ton loading frame with a four-point loading system. In the middle of the specimen, a loading jack held the load cell. A hydraulic pump with a manual system was used for loading of specimens. The measurements of deflection and strain values were recorded with a help of an LVDT and a data logger.

The breadth of a fracture in a specimen was measured using a portable microscope with an optical amplification factor of 40 and a sensitivity of 0.01mm. A theodolite device fixed above a specimen support measured end rotation with an accuracy of 20 seconds. A measurement staff gauge measured vertical deflection with a reading placed at a fixed distance from a specimen.

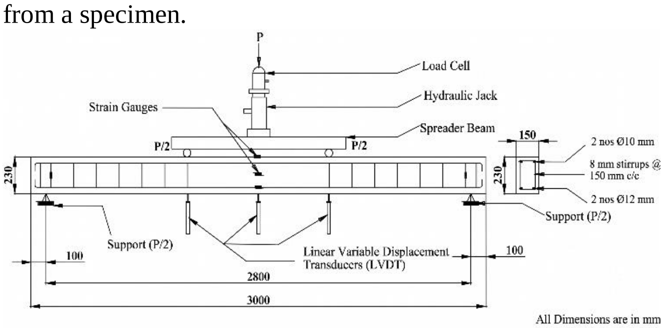

(a)

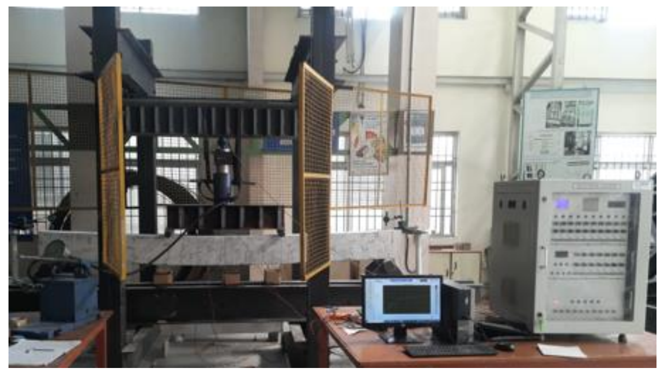

(b)

Fig. 5 (a) Diagram showing the test configuration for the GPC beams, and (b) Flexural strength testing apparatus.

5. Discussion of Experimental Results

5.1. Bond Strength

The effectiveness of anchoring in reinforced bars and effective lap splices, which directly affect the ultimate load-carrying capacity of RC structures, depends critically on the bond stress factor. The bond tension between the reinforcement and concrete is influenced by the geometric features of deformed bars, which are most often utilized as reinforcement in contemporary concrete constructions.

Rib height, rib spacing, inclination, and general rib geometry are the most relevant parameters to the mechanical interlock of both materials, concrete and rebar, and therefore to the development of bond resistance during loading. Previous studies [43, 44] have shown that changes to these geometrical parameters alter the mechanisms of stress transfer at the rebar–concrete interface and hence affect both the initial stiffness and the maximum bond strength.

For the best performance of bond strength, it is very essential that adhesion, friction, and mechanical interlock are well-integrated. A proper balance among these mechanisms ensures that the bar develops sufficient anchorage before large slip occurs. The test was carried out by measuring the relative displacement continuously from concrete and the reinforcing bar during incremental loading. These measured displacements, representing the progression of slip and damage in bond, have been plotted and presented in Figures 6 (a-c) for detailed observation and comparison.

5.1.1. Relation between Bond Strength, Pull-Out Load and Size of Steel Bar

The obtained BS values from different GPC mix proportions showed a marked reverse relation with the diameter of the rebars, thus implying that smaller rebars are allied with higher resistance bond performance. For GPC mix proportions GP30M4, GP50M4, and GP70M4 with concealed reinforcement, empirical analysis indicated increased bond strength of 3.82%, 5.61%, and 6.51%, respectively, when 12 mm rebar was replaced by a 10mm rebar. A similar trend is observed in mix proportions without concealed (WOC) reinforcement, where GP30M4, GP50M4, and GP70M4 mix proportions indicated increased bond strength of 3.68%, 5.36%, and 5.76%, respectively, after decrementing rebar diameter. The above findings support the proposition that smaller-diameter rebars are better at achieving effective mechanical interlock and exemplary capability of effective stress transfer in the rebar-concrete interface. The total pull-out load values, along with BS results, for all GPC mix proportions with both 10mm and 12mm rebars, are presented in Tables 6 & 7 below, thus providing an all-encompassing analysis of bar diameter influence on GPC bond performance.

The experimental outcomes revealed that the ultimate loads are higher in specimens using 12 mm rebars compared to specimens using 10 mm rebars. With regards to the effects of the deformed reinforcement, BS primarily stems from the mechanical interlock mechanism sustained by the ribs on a reinforcing bar and the surrounding cementitious matrix. As a function of an increased rebar diameter, both bond area & bond depth available for mechanical interlock increase, thus increasing the ultimate load-bearing capacity despite a reduction in BS under equal circumstances. Such effects make it feasible for the specimen to withstand an increased level of ultimate load, despite the BS being reduced under equal circumstances because of a higher surface area in direct interaction. Similar effects have been reported in earlier studies, discussed under References [45, 46].

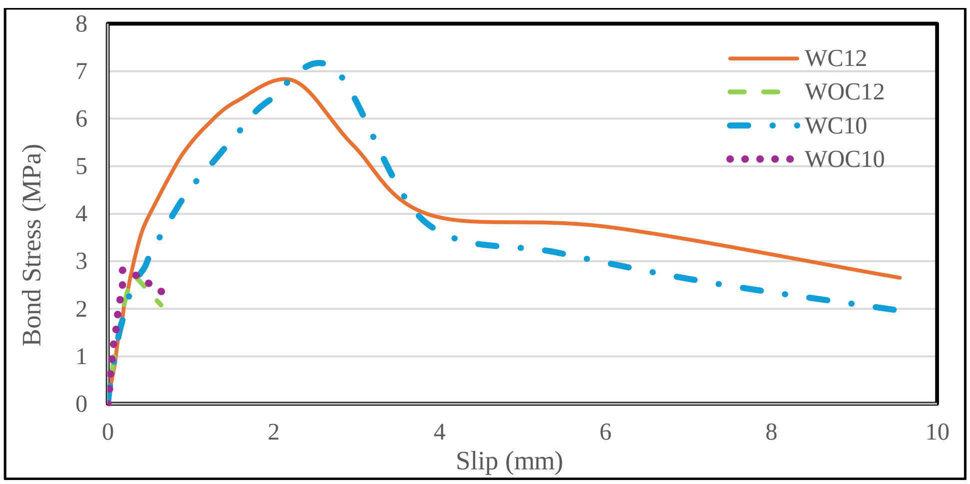

(a)

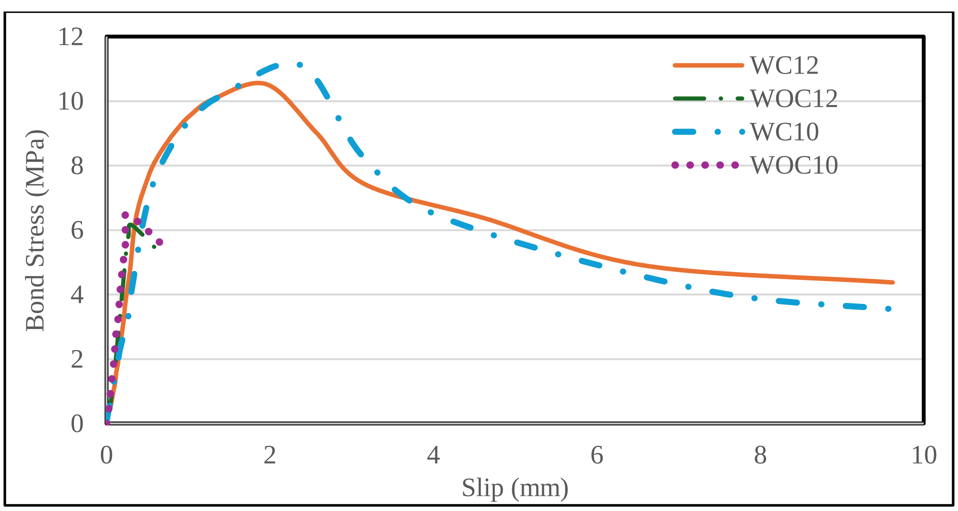

(b)

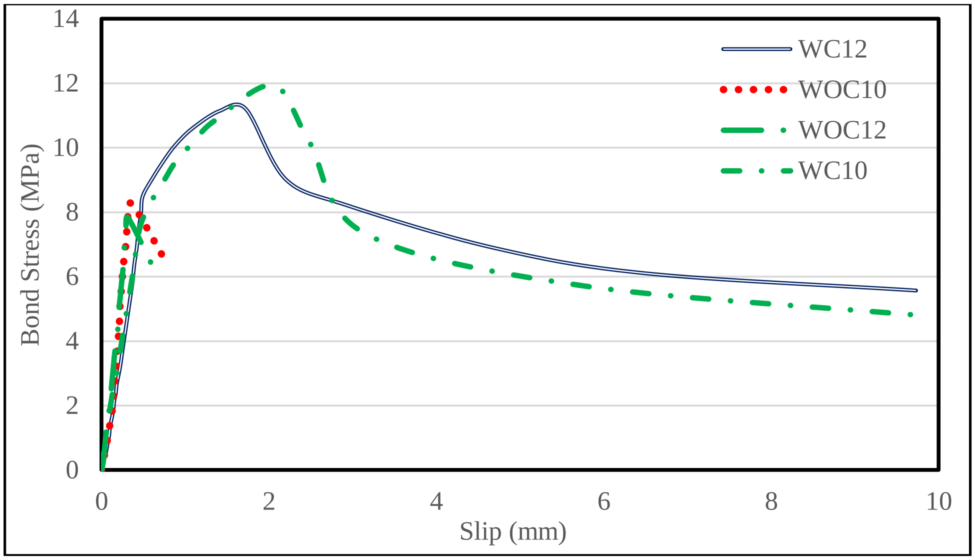

(c)

Fig. 6 (a) Bond stress–slip relationships of mix GP30M4 with rebars of both 12 mm and 10 mm in diameter, (b) Graph showing bond stress with respect to slip for GP50M4 mixture with both 12mm and 10mm rebars, (c) Graph of bond stress and slip for GP70M4 mix using rebars that are 10 mm and 12 mm in diameter.

Table 6. Effect of concealed reinforcement on the ultimate load and bond strength of GPC mixes

Mix ID	**GP30M4**		**GP50M4**		**GP70M4**	
Diameter of bar d_r (mm)	12	10	12	10	12	10
Ultimate load P (kN)	25.64	22.18	39.67	34.91	42.27	37.5
Ultimate bond stress τ (MPa)	6.80	7.06	10.52	11.11	11.21	11.94

Table 7. Displays the final load and bond strength values for the WOC reinforcement of GPC mixtures

Mix ID	**GP30M4**		**GP50M4**		**GP70M4**	
Diameter of bar d_r (mm)	12	10	12	10	12	10
Ultimate load P (kN)	10.24	8.86	23.22	20.38	29.44	25.95
Ultimate bond stress τ (MPa)	2.72	2.82	6.16	6.49	7.81	8.26

5.2. General Observations of Flexural Behavior of GPC

The flexural behavior shown by all the beams was essentially structural. There are no horizontal cracks in the reinforcement area; this implies that there was no bond failure between the GPC and the reinforcement. Vertical flexural cracks were observed with a high degree of ultimate deflection in the constant moment zone. Because the SRBs were intended as under-reinforced sections, the tensile reinforcement yielded in the pure bending zone. Based on these observations, it can be concluded unequivocally that GP30M4 behaves similarly to GP50M4 and GP70M4 concrete. The observations made collectively indicate that the behavior of reinforced GP30M4, GP50M4, and GP70M4 beams is similar to other GPCs prepared using FA, biomedical waste ash, GGBS, dolomite, MK, WGP as fine aggregates, hybrid fibres (comprising crimped steel and polypropylene fibres), as well as CFRP and GFRP bars [22-26].

5.2.1. Ultimate Loads Behavior of GPC Beam

Tables 8 & 9 below show the load-carrying capacity & moment-carrying capacity for the beam, theoretically and experimentally determined & reinforced for the service load stage & ultimate load stage, respectively. Compared to the load-carrying capacity & moment-carrying capacity for the GP70M4 reinforced beam, the values for the GP30M4 reinforced beam are lower for both. Compared to the load-carrying capacity & moment-carrying capacity for the ultimate load of the GP70M4 beam, those for the GP30M4 beam are lower. The load-carrying capacities are higher in the GP70M4 beam by 8.79% than in the GP30M4 beam. Moreover, the load-carrying capacities in the GP50M4 beam are higher by 5.71% in contrast to the GP30M4 beam's load-carrying capabilities. The moment-carrying capacities in the GP70M4 beam are higher by 2.91% compared with the moment-carrying capacities in the GP50M4 beam. Additionally, it was observed that the incorporation of a higher silica fume concentration of 5M in the GPC increases the beam's capacity to support loads and moments for the service and ultimate loading phases by 5.71% and 8.79%, respectively. Moreover, GP70M4-reinforced beam withstands much higher deflection and bears a much greater load. The stress block analysis approach was used to estimate the theoretical design moment of the beams as stated in the code of BS 8110 [47] and IS 456:2000 [42]. The results revealed that the ultimate moments determined from the experimental methods were found to be around 13–16% higher in the case of GPC beams with a reinforcement ratio of 0.79%. The results showed that both BS 8110 [47] and IS 456:2000 [42] can be applied to estimate the conventional ultimate moment capacity of the GPC beam. This estimation remains valid for reinforcement ratios up to 0.79%, provided that an appropriate load factor is used to account for failure conditions. The beam-test outcomes were then evaluated by comparing them with findings from other studies on GPC beams listed in Table 6 [17, 20, 21, 28, 30-32]. Overall, it is clear that the conclusions of the present study are consistent with those reported in earlier research by other investigators.

Table 8. Lists the theoretical and experimental values for the moment and load during the service stage

Beam ID	Experimental values		Theoretical values		Capacity ratio (Exp/Theo)
	Moment (kNm)	Load (Tonnes)	Moment (kNm)	Load (Tonnes)	
GP30M4	13.88	3.03	12.23	2.67	1.13
GP50M4	14.67	3.21	12.73	2.78	1.15
GP70M4	15.10	3.30	13.02	2.84	1.16

Table 9. Theoretical and experimental moment and load values in the final Stage

Beam ID	Experimental values		Theoretical values		Capacity ratio (Exp/Theo)
	Moment (kNm)	Load (Tonnes)	Moment (kNm)	Load (Tonnes)	
GP30M4	20.82	4.55	18.35	4.01	1.13
GP50M4	22.01	4.81	19.10	4.17	1.15
GP70M4	22.65	4.95	19.53	4.27	1.16

5.2.2. Deflection Behavior of GPC Flexure Beam

The deflection at the point of loading and mid-span LVDT was used to measure the beam. The findings that were achieved, which were subsequently graphed using a load-deflection curve in Figures 7 (a, b), are indicated in Table 9 above. A uniform load-deflection curve was observed for all tested beams. Before the appearance of a crack in the beam, load-deflection curve behavior indicated a gradual and linear trend. The beam's mid-span deflection reduced with increased stiffness in 3.5M mix GP30M4. After the appearance of a crack in the beam, all beams showed nonlinear behavior. The GP70M4 reinforced beam indicated a higher capacity in withstanding deflections at the ultimate load stage compared to GP30M4 and GP50M4 in GPCs. Therefore, the addition of SF contributes to an increase in stiffness indicated by load-deflection curve behavior. The GP70M4 beam can withstand higher deflections compared to GP50M4 and GP30M4 during service and ultimate load stages. During the yield stage, GP70M4 can withstand a deflection of 9.24mm at mid-span, which shows a reduction of approximately 10.64% from the GP30M4 beam. At the ultimate load stage, GP70M4 withstood a mid-span deflection of 44.84 mm, which shows nearly a 17.57% increase compared to the GP30M4 beam. Ultimate deflection at the load point for GP70M4 was recorded to be 34.85 mm, this indicates a 9.49% increment as compared to that of the beam of GP30M. However, in contrast, the ultimate deflection at load point for GP50M4 measured 33.61 mm, which shows an approximate increase of 5.59% from GP30M4. However, based on standards IS-456:2000 [42] and BS-8110 [47], a permitted span/250 deflection shows the necessity for conformity with aesthetic & safety requirements. Hence, a need arises for increased depths of a beam with increased concrete & load-carrying capacity. Additionally, it is relevant to point out that currently conducted tests are limited to short-term loading situations and do not take into consideration creep effects such as shrinkage. In subsequent phases, load-deflection curve measurements recorded considerable deflections with very small additions in load. Worth mentioning is the fact that GP30M4 beam behavior corresponds to GP50M4 and GP70M4, in addition to other GPC beams [17, 20, 21, 27, 28, 32].

5.2.3. Ductility Characteristics of GPC Beams

The study of displacement ductility formed a major part of the research. The ductility ratio of the studied GP30M4, GP50M4, and GP70M4 beams is recorded in Table 10. The expression of the ductility ratio as proposed by the ACI committee is written as $\mu = (\Delta u / \Delta y)$, in which Δu = carries the beam's final displacement. Meanwhile, Δy = denotes the yield displacement. The high ductility ratio of the beam portrays its ability to sustain high deflections prior to failure. According to the findings proposed by Shuaib HA et al. in 1991 and supported by another research sponsored by Ashour et al. in 2000, a beam ought to have a displacement ductility ratio between 3 and 5 in order to possess high ductility and adequate moment distribution [48, 49]. The results of the proposed study show that every tested beam exceeded a displacement ductility ratio of 3. The GPC with a 5M NaOH concentration and 5% SF clearly had a greater displacement ductility ratio than the GP30M4 reinforced GPC beam. The GP50M4 and GP70M4 displacement ductility ratios showed 19.24% and 44.17% increases from that of the GP30M4 displacement ductility ratio, respectively.

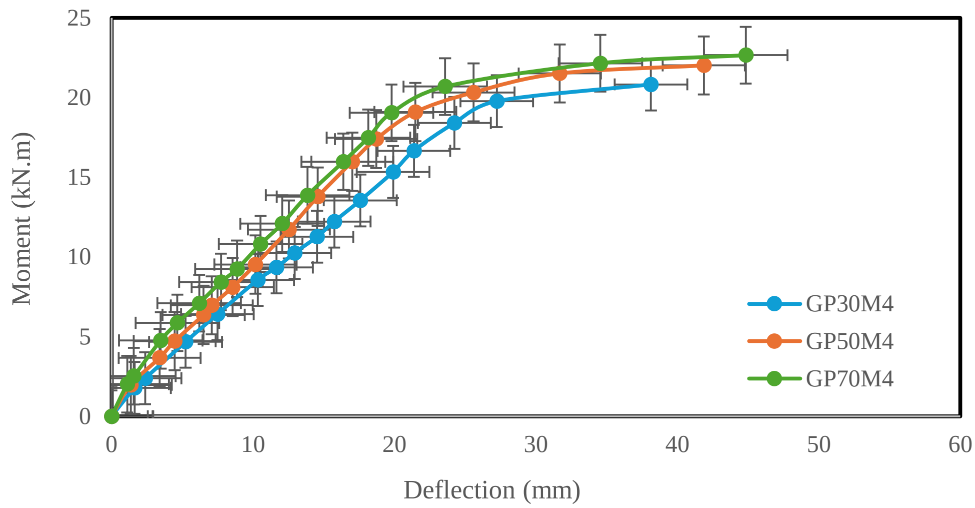

(a)

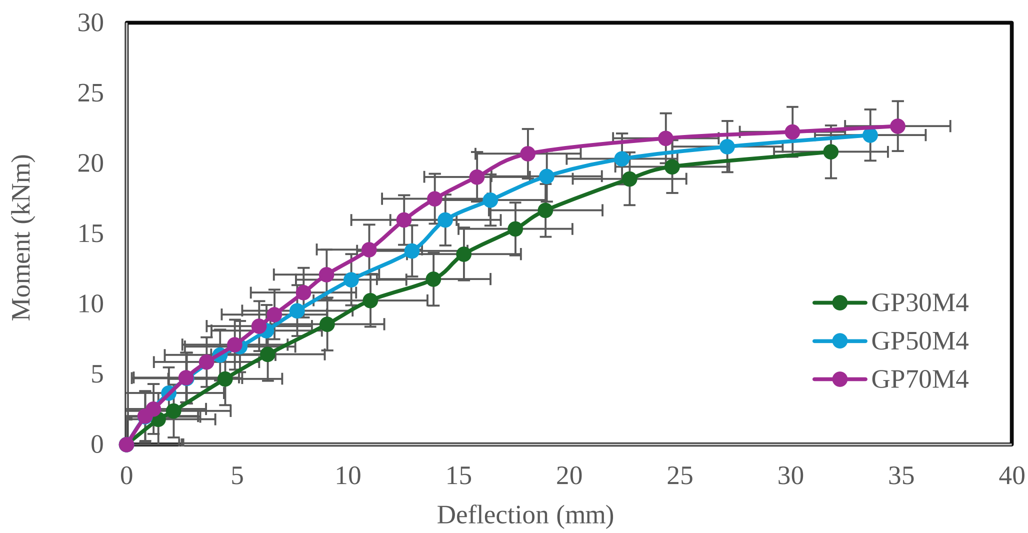

(b)

Fig. 7 (a) Moment vs. Deflection at Mid-span, and (b) Ultimate moment versus at the loading point, deflection.

According to existing literature proposed by different studies and sponsored by several organizations within different research studies on the topic, a displacement ductility ratio of 3 to 5 bears adequate displacement ductility aptly apt to be applied in displacement-based structures such as those subjected to seismic activity [49].

Table 10. Experimental Moment versus GPC Beam Deflection

Beam ID	Displacement at the Yield phase (Δy)		Ultimate load stage displacement at Mid-Span (Δu)		Displacement ductility ratio (μ)=(Δu)/(Δy)
	Moment (kN.m)	Deflection (mm)	Moment (kN.m)	Deflection (mm)	
GP30M4	8.55	10.34	20.59	38.14	3.69
GP50M4	10.18	9.52	21.97	41.88	4.40
GP70M4	8.88	9.24	22.83	44.84	4.85

5.2.4. Cracking Behavior of GPC Beam

The development of crack initiation in loaded beams is also marked using a marker. Observation shows that the first crack developed near the loading position, shown in Figure 8. An initial crack load is considered where linearity is lost on load-deflection curves. The special characteristics of crack development in reinforced GPC beams are compiled in Table 10. It is evident that the beam has developed vertical fissures on its surface, indicating bending-related collapse. In this study, it is found that a smaller number of cracks is associated with higher strength GPC, shown in Figures 8 (a-c). Number of cracks developed between loading points in GP30M4, GP50M4, and GP70M4 beams is recorded as 13, 10, and 9, respectively. Spacing of the crack developed in GPC beams varies in between 90.76 mm to 102.53 mm. Width of the maximum crack developed in GP30M4, GP50M4, and GP70M4 beams is measured as 0.06, 0.08, and 0.1 mm, respectively. The presence of a broad crack in a beam greatly reduces their rigidity, assisting the entrance of harmful materials. According to the IS 456:2000 [42] and BS 8110 [47] codes, the width of cracks must not be more than 0.3 mm, considering the exposure condition. In this investigation, the crack widths of all beams were less than 0.3 mm. The GP50M4 and GP70M4 beams showed higher load-carrying capacity than the GP30M4 beams after the appearance of initial cracks. The flexural cracks due to constant moment developed in the vertical upward direction and showed a gradual increase in width with increased load.

The width of the cracks developed in each incremental load at the level of the tensile rebars in the GPC beams was quantitatively investigated, and the development of the cracks was demarcated on the GPC beam. At the initial stages of the GP30M4, GP50M4, and GP70M4 GPC beam failures, the initial cracks occurred at about 41.09%, 50.98%, and 38.79% of the final load of the GPC beams, respectively. It can be noted that the first crack in the GP70M4 GPC beam failed at a lower percentage of the final loading. Each GPC beam failure, the initial fracture was formed near the middle part of the beam. Vertical cracks were seen on the surfaces of the GPC beam. Hence, one can conclude that the failure mechanism of the GPC beam is flexural. The results of the initial fracture of the GPC beam can be viewed in Table 11. The phrase "moment of the first crack" is the position of the visible change of the graph curve of the moment of curvature. To effectively work, it is imperative that the GPC beam will not have excessive cracks. The influence of excessive cracks on the GPC beam will significantly reduce the stiffness of the GPC beam to accommodate the entry of harmful substances into the concrete mixture. The results show that the widths of the cracks in the GPC beam due to the action of the service loads remained well below the maximum permissible values given in IS 456:2000 [42] and BS 8110 [47]. The values given in the code depict a reasonable approximation of the widths with fair accuracy. The crack spacing's average value in GPC beam is 90mm, 97mm, and 102mm in the GP30M4, GP50M4, and GP70M4 GPC beam, respectively. The value matches the GPC determinations found in the existing literature on GPCBs results [17, 25, 28, 31].

5.2.5. Concrete and Steel Strain Behavior

For each loading phase, the strain created in the concrete (compression strain) and steel (tension strain) was measured. Figures 9 (a-c) shows the moment vs. compressive strain, moment vs. tension strain, and movement vs. tension strain at stirrups. Before failure, the compressive strain of the reinforced GPC beam GP30M4, GP50M4 and GP70M4 was in the range of 0.0018–0.0021 and 0.0023.

Fig. 8 (a) Formation of crack pattern of GP30M4 mix GRC beam

Before failure, the tension strain of the reinforced GPC beams GP30M4, GP50M4 and GP70M4 was in the range 0.00247, 0.00229 and 0.00212. Before failure, the tension strain at the stirrups of the reinforced GPC beams GP30M4, GP50M4 and GP70M4 was in the range of 0.00182, 0.00162 and 0.00144. After cracking, the tension strain of the GP70M4 and GP50M4 beam was lower than GP30M4 reinforced GPC beam. Greater steel strain and a large deflection close to the collapse, with noticeable broadening, were signs that the beam had failed.

Table 11. Cracking characteristics for GPC flexure specimens

Beam ID	Crack width at the moment of service (mm)	Crack width at the ultimate moment (mm)	Allowable crack width according to IS:456–2000 (mm)	Average distance between cracks (mm)	The quantity of cracks between the load points
GP30M4	0.06	1.64	0.3	90.76	12
GP50M4	0.08	1.16		97.54	10
GP70M4	0.1	0.82		102.53	9

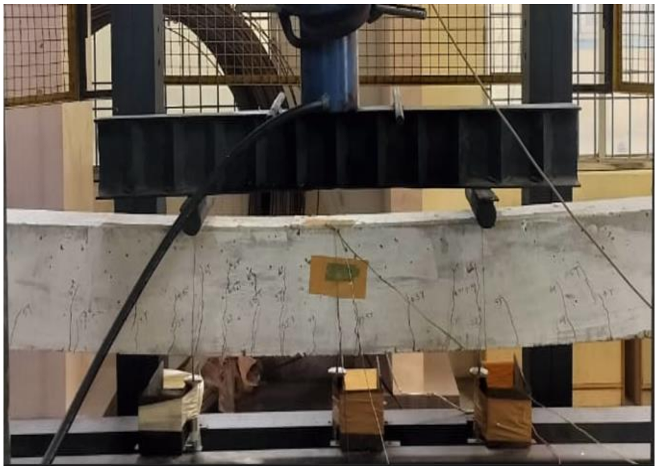

Fig. 8 (b) Formation of Crack pattern of GP50M4 mix GRC beam

Fig. 8 (c) Formation of Crack pattern of GP70M4 mix GRC beam

The failure zone of the GP70M4 beam was higher than GP30M4 reinforced GPC beams. As a result, the longitudinal reinforcement deformed specifically at the location of the crack, and the reinforcement bar ruptures once it reached its ultimate state, along with an abrupt reduction in load. The current study yields the same outcomes just like the previous researchers [50-52]. As such, GP30M4 is able to attain the strain capacity under the action of the flexural loading. However, the failure region of GP30M4 was larger compared to the GP50M4 and GP70M4 beam, as given in Figure 8 (a-c).

5.2.6. End Rotation of the GRC Beams

The end rotation of the beam is an important parameter for the analysis of curvature of structural components. Graphs showing moment versus end rotation for singly reinforced GP30M4, GP50M4, and GP70M4 GPC beams are presented in Table 12 and Figure 10. Graph showing moment vs. end rotation for singly reinforced GPC beams follows a standard behaviour of such graphs, linear until the steel's yield point is reached. End rotation of GP30M4, GP50M4, and GP70M4 was noted to be between 1°10'48" & 3°10'12", 1°03'36" & 3°43'12", & 0°51'36" & 4°02'24", respectively. Following the concrete break in the tension zone, the major share of the tension part of the moment was taken over by the steel reinforcement. With the increase in angular displacement of the beam, the stresses in the reinforcement increased proportionally. Eventually, the yield stress in the steel was reached at one or multiple points. Eventually, the steel yields. Almost immediately after yielding begins, large increases in the terminal rotations take place. This is in agreement with other researchers' results found in [50, 53]. Figure 11 shows the tested beam specimens in the laboratory.

Table 12. End rotation of GPC flexural beam

Beam ID	Moment at service stage (kNm)	Moment at ultimate stage (kNm)	End rotation service stage (º)	End rotation at ultimate stage (º)
GP30M4	13.88	20.82	1º10'48"	3º10'12"
GP50M4	14.67	22.01	1º 03'36"	3º43'12"
GP70M4	15.10	22.65	0º51'36"	4º 02'24"

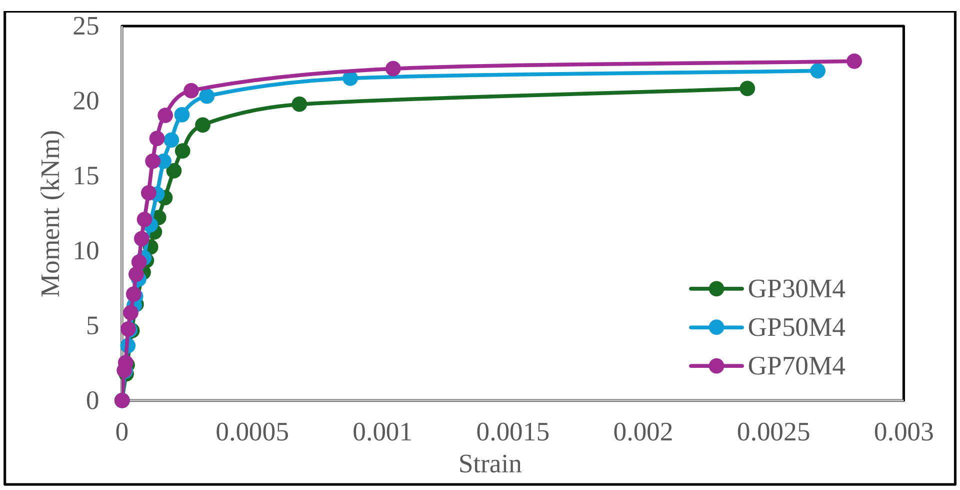

(a)

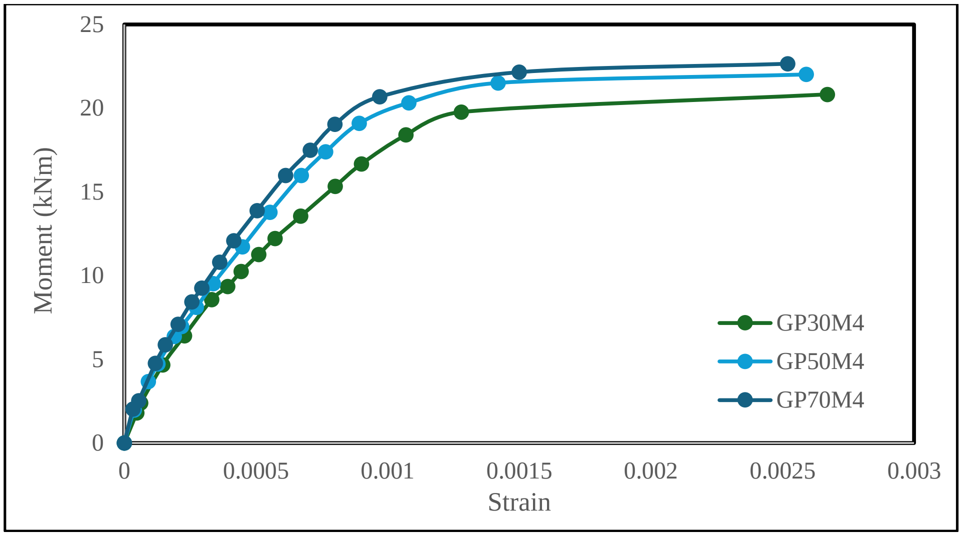

(b)

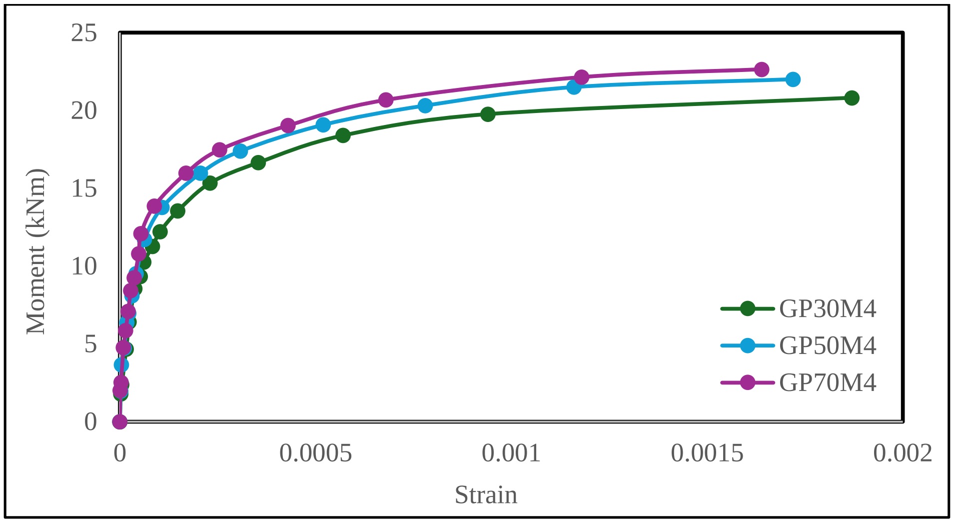

(c)

Fig. 9 (a) Moment vs compressive strain in midspan of GPRC beams,
(b) Moment versus tension strain in midspan of GPRC beams, and (c) Moment versus strain in stirrups.

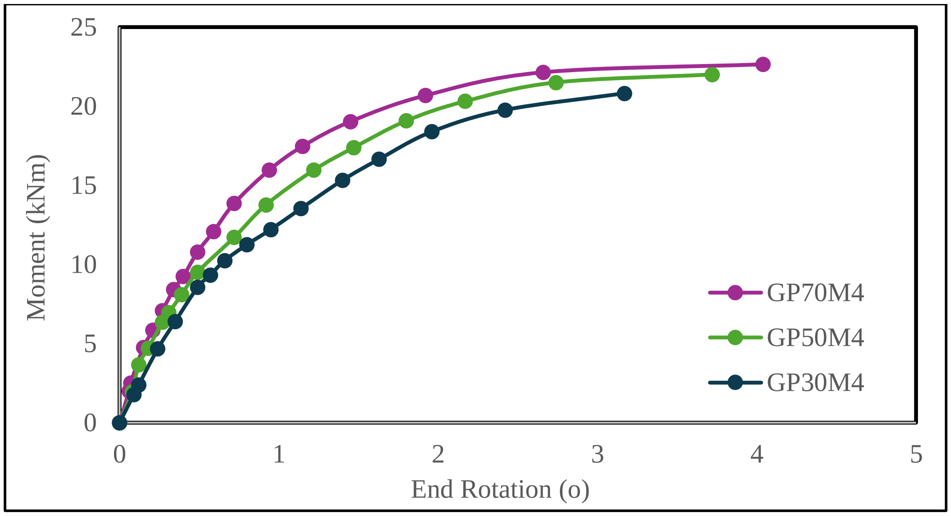

Fig. 10 End rotation terminal rotation

Fig. 11 Tested GPC beams of GP30M4, GP50M4 and GP70M4 mixes

6. Microstructural Characterization

6.1. Analysis of SEM/EDAX spectrum

The related EDAX analysis and SEM images of the GP30M4, GP50M4, and GP70M4 specimens at different magnifications are presented in Figures 12 to 14. N-A-S-H and C-A-S-H gels are some of the gel phases identified on the surface of all GP matrix specimens through the SEM images. They are formed due to the alkali-induced FA and GGBS reactions in which some unreacted FA particles are involved.

Moreover, the SEM images revealed that spherical FA particles are in the process of dissolving and that the dissolved particles appear to be part of the gels. This same phenomenon is evident in the SEM images of 200 µm where the occurrence of simultaneous and sequential reactions is evidenced.

In addition, the SEM images reveal the presence of some unreacted particles. Compared to GP30M4 and GP50M4, GP70M4 has the highest gel phases in the mixes under study. The EDAX results of GP matrix confirm the presence of Ca, Si, Al, O, Fe, and Na elements in the composition, with different intensities of signals in the mixes.

This study has confirmed the formation of N-A-S-H type and C-A-S-H type gels. Since the concentration of Na and Al is nearly equal, GP30M4 has a Na/Al ratio of 1 where one Na^+ ion is able to balance each aluminum ion, which is a balanced situation for all the mixes. However, the Si/Al ratio of GP50M4 and GP70M4 mixes is greater than 1, although the ratio of GPC is less than 1.

These observations demonstrate that gel formation and the development of the gel network are strongly affected by the increasing molarity of the alkali solution as well as by the incorporation of SF. For GP50M4, raising the molarity of the alkali solution accelerates the dissolution process, increases the reactivity, and prolongs gel formation, which ultimately results in a more pronounced binding character and a consequent increase in strength. For GP70M4, the addition of SF and increased molarity of alkali solution will affect the reactive entities in the blend, increasing the extent of gelation, strength, and binding capabilities. These results are in agreement with the literature concerning CS [54].

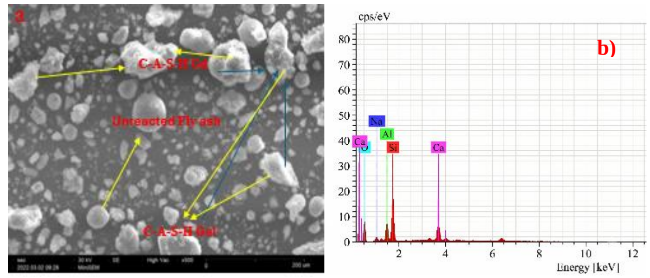

Fig. 12 (a) SEM micrograph (200 µm), and (b) EDAX spectrum of the GP30M4 mix.

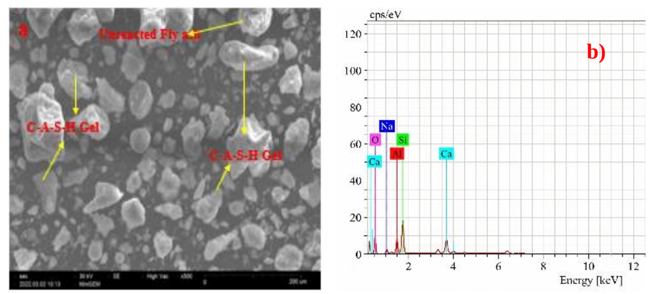

Fig. 13 (a) SEM micrograph (200 µm), and (b) EDAX spectrum of the GP50M4 mix.

6.2. Analysis of XRD

The XRD spectra of GP30M4, GP50M4 and GP70M4 are illustrated in Figure 15. Amorphous gel phases are seen in all GPC mixtures between 20° and 28° 2θ values. The 2θ value of 24° contains the semi-crystalline hydroxysodalite, which is more noticeable and intense in GPC12. The presence of more reactive silica from SF may be the cause of this.

In the end, more gel formation raises the strength values, which are associated to the CS outcomes. In every instance, the C-S-H gel is present at 28° and 29° 2θ values. The XRD data, which are comparable to those reported by Nagsjothi et al. [55], show the gel formation and influence of SF in the GP. In FA and GGBS, the unreacted crystalline phase is still present as quartz, akermanite, and gehlenite.

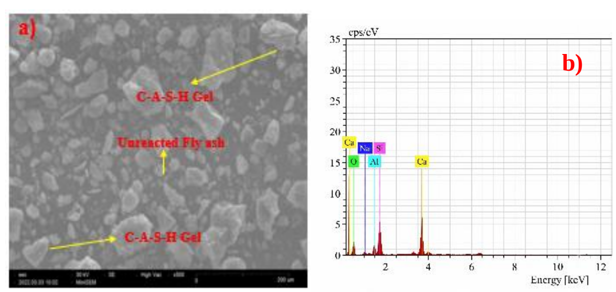

Fig. 14 (a) SEM micrograph (200 µm), and (b) EDAX spectrum of the GP70M4 mix.

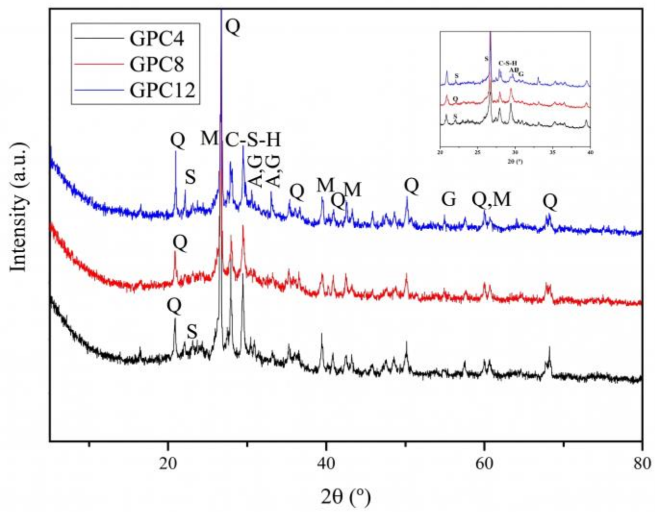

Fig. 15 Comparative XRD patterns of GP30M4, GP50M4, and GP70M4 mixes.

7. Conclusion

Several trials were conducted in order to investigate technical feasibility of concrete mixtures incorporating various industry by-products like FA and GGBS, strength of alkali liquid solution, and the simultaneous partial FA substitution with SF admixture in GP30M4, GP50M4, and GP70M4 series of GPC were studied. The following inferences can be deduced from the experimental outcomes in connection with bond stress and static flexural specimens.

- The ultimate bond strength of Without Concealed (WOC) GPC specimens failing by concrete splitting increased in concrete CS, but a reverse trend was observed with an increase in rebar diameter.
- In case of GP30M4, GP50M4, and GP70M4 mix with concealed reinforcement, based on experimental results, an increase in bond strength of 3.82%, 5.61%, and 6.51%, respectively, was observed with the substitution of a 12 mm rebar with a 10 mm rebar.
- The flexural performance of GPC is analogous to GP and cement concretes.
- The standard behaviour of a structure under flexure was monitored in all the beams, was observed, with no horizontal cracks identified to disclose a lack of bond failure. In addition to providing a sufficient safety factor against failure, both British Standards BS 8110 and IS 456:2000 may be used to provide a safe ultimate moment of resistance for reinforcing amounts not exceeding 3.14%.
- The amount of deflection that the design service causes load can be considered satisfactory since it is within safe limits in accordance with BS 8110 and IS 456:2000. The GP70M4 beams performed quite well in terms of ductility. The GPC beams' fractures ranged in width from 0.06 mm to 0.1 mm, which is within acceptable bounds.
- The GP30M4 mix blend also successfully achieved its full-strength potential when subjected to bending loads.
- The end rotations of GP30M4 beams before failure were approximately equal to those of GP50M4 & GP70M4 mix.
- The microstructure study supported the 5% SF addition because raising the NaOH content altered the reactive species in the medium, which accelerated the reaction rate. In SEM, the GP70M4 and GP50M4 samples show a denser gel. For the GP50M4 and GP70M4 mixtures, the hydroxy sodalite peak's intensity rose in XRD.

A hypothesis can be formed in which GPC will become a preeminent surrogate for conventional cement concrete. With a deeper comprehension of bond stress behaviour and static flexibility, it is established in this research that low concentration alkali-activated GP30M4, GP50M4, and GP70M4 grades of GPCs could be achieved for precast units. In subsequent research, the usage of these mixes of GPCs will prove to be highly useful in precast units, road construction, pavement works and designing high performance concretes, which will in turn lead to the development of an eco-friendly construction material. Future studies will include research on mix designs for one-part GPCs, with a study of their mechanical properties, durability, life cycle analysis, and viability for construction.

Acknowledgement

We would like to thank Centre for Advanced Concrete Research – Civil (CACR – Civil), Structural Testing lab, Department of Civil Engineering, SRM Institute of Science and Technology, Kattankulathur, for their support in carrying out the research work.

Disclosure statement

Concerning the writing and publishing of this research paper, the authors reported no conflicts.

Funding Declaration

No funding was received to assist with the preparation of this manuscript.

Author Contribution

Baskara Sundararaj J - Conceptualisation, Methodology, Formal analysis, Validation, Investigation, Writing – Original Draft; Kannan Rajkumar P R - Supervision, Resources, Writing - Review & Editing

References

[1] Hemn Unis Ahmed et al., "Geopolymer Concrete as a Cleaner Construction Material: An Overview on Materials and Structural Performances," *Cleaner Materials*, vol. 5, pp. 1-18, 2022. [CrossRef] [Google Scholar] [Publisher Link]

[2] Adeyemi Adesina, "Recent Advances in the Concrete Industry to Reduce its Carbon Dioxide Emissions," *Environmental Challenges*, vol. 1, pp. 1-8, 2020. [CrossRef] [Google Scholar] [Publisher Link]

[3] Fred Andrews-Phaedonos, "Geopolymer "Green" Concrete – Reducing the Carbon Footprint – The VicRoads Experience," *8th Austroads Bridge Conference*, Sydney, NSW, Australia, pp. 386-396, 2011. [Google Scholar]

[4] Ahmad L. Almutairi, "Potential Applications of Geopolymer Concrete in Construction: A Review," *Case Studies in Construction Materials*, vol. 15, pp. 1-20, 2021. [CrossRef] [Google Scholar] [Publisher Link]

[5] Peiliang Cong et al., "Comparison and Assessment of Carbon Dioxide Emissions between Alkali-Activated Materials and OPC Cement Concrete," *Journal of Traffic and Transportation Engineering (English Edition)*, vol. 11, no. 5, pp. 918-938, 2024. [CrossRef] [Google Scholar] [Publisher Link]

[6] Amer Hassan, Mohammed Arif, and M. Shariq, "Use of Geopolymer Concrete for a Cleaner and Sustainable Environment–A Review of Mechanical Properties and Microstructure," *Journal of Cleaner Production*, vol. 223, pp. 704-728, 2019. [CrossRef] [Google Scholar] [Publisher Link]

[7] Parah Salsabeel Jalal, Vikas Srivastava, and A. K. Tiwari, "Geopolymer Concrete: An Alternative to Conventional Concrete for Sustainable Construction," *Journal of Environmental Nanotechnology*, vol. 13, no. 4, pp. 218-225, 2024. [CrossRef] [Google Scholar] [Publisher Link]

[8] Rania Emara et al., "Geopolymers as Sustainable Alternates for Portland Cement in Constructive Concrete: Systematic Review," *Alexandria Journal of Science and Technology*, vol. 2, no. 2, pp. 90-103, 2024. [Google Scholar] [Publisher Link]

[9] Arun Parashar et al., "Regression and Cluster Analysis of GGBS based Geopolymer Compositeat Different Proportion of Ceramic Dust," *Indian Journal of Engineering and Materials Sciences (IJEMS)*, vol. 30, no. 6, pp. 747-756, 2023. [CrossRef] [Google Scholar] [Publisher Link]

[10] Arun Kumar Parashar, and Nakul Gupta, "An Investigation of Micro-Silica Inclusion in Slag-based Geopolymer Concrete with Regression and Cluster Analysis," *Asian Journal of Civil Engineering*, vol. 24, no. 8, pp. 3759-3765, 2023. [CrossRef] [Google Scholar] [Publisher Link]

[11] Jacqueline Obeng et al., "Bond Behavior of Reinforcing Steel Bars in Metakaolin – Calcium Carbide Residue-based Geopolymer Concrete," *Engineering Research Express*, vol. 6, no. 3, 2024. [CrossRef] [Google Scholar] [Publisher Link]

[12] Tuan Anh Le, Thuy Ninh Nguyen, and Khoa Tan Nguyen, "Experimental, Numerical, and Theoretical Studies of Bond Behavior of Reinforced Fly Ash-Based Geopolymer Concrete," *Applied Sciences*, vol. 12, no. 15, pp. 1-19, 2022. [CrossRef] [Google Scholar] [Publisher Link]

[13] Vincenzo Romanazzi, Marianovella Leone, and Maria Antonietta Aiello, "Bond Performance of Geopolymer Concrete with Steel and FRP Reinforcements," *Journal of Composites Science*, vol. 9, no. 6, pp. 1-22, 2025. [CrossRef] [Google Scholar] [Publisher Link]

[14] Maria Antonietta Aiello et al., "Bond Behavior of Geopolymer Concrete with CFRP and GFRP Bars," *Proceedings of Italian Concrete Conference 2022*, Naples, Italy, pp. 94-103, 2022. [CrossRef] [Google Scholar] [Publisher Link]

[15] Padakanti Rakesh et al., "A Comparative Study on Bond Behavior of Ternary Blended Geopolymer Concrete and Conventional Concrete," *Low Carbon Materials and Technologies for a Sustainable and Resilient Infrastructure Conference Paper*, pp. 459-470, 2023. [CrossRef] [Google Scholar] [Publisher Link]

[16] R. Nurwidayati et al., "Effect of Embedment Length on Bond Strength of Geopolymer Concrete," *AIP Conference Proceedings: Proceedings of Advanced Material, Engineering & Technology*, Seoul, South Korea, vol. 2291, no. 1, 2020. [CrossRef] [Google Scholar] [Publisher Link]

[17] Yuanzheng Lin et al., "Flexural Behaviour of Reinforced One-part Geopolymer Concrete Beams," *Journal of Building Engineering*, vol. 96, 2024. [CrossRef] [Google Scholar] [Publisher Link]

[18] Banu D. Handonoa et al., "The Evaluation of Behavior of Geopolymer Reinforced Concrete and Conventional Reinforced Concrete Beams: A Critical Review," *Research on Engineering Structures and Materials*, vol. 9, no. 4, pp. 1433-1457, 2023. [CrossRef] [Google Scholar] [Publisher Link].

[19] Xiangsheng Deng et al., "Experimental and Theoretical Study on the Effects of Stirrup Ratio and High Temperature on BFRP-Reinforced Geopolymer Concrete Beams," *Journal of Building Engineering*, vol. 117, pp. 1-27, 2026. [CrossRef] [Google Scholar] [Publisher Link]

[20] Muhammad Sigit Darmawan et al., "Comparative Study of Flexural Performance of Geopolymer and Portland Cement Concrete Beam Using Finite Element Analysis," *International Journal of Geomate*, vol. 23, no. 95, pp. 1-9, 2022. [Google Scholar] [Publisher Link]

[21] Hala Mamdouh et al., "Effects of Size and Flexural Reinforcement Ratio on Ambient-Cured Geopolymer Slag Concrete Beams under Four-Point Bending," *Buildings*, vol. 12, no. 10, pp. 1-17, 2022. [CrossRef] [Google Scholar] [Publisher Link]

[22] Basanth Babu K. Mohanram, and Ramesh Kanagavel, "Effect of Metakaolin on Mechanical Properties and Flexural Behavior of Geopolymer-Reinforced Concrete Beams," *Practice Periodical on Structural Design and Construction*, vol. 27, no. 3, 2022. [CrossRef] [Google Scholar] [Publisher Link]

[23] P. Saranya et al., "Flexural Behaviour of GGBS-Dolomite Geopolymer Concrete Beams under Cyclic Loading," *Materials Science Forum*, vol. 969, pp. 291-296, 2019. [CrossRef] [Google Scholar] [Publisher Link]

[24] A. Suresh Kumar, "Flexural Behaviour of Reinforced Geopolymer Concrete Incorporated with Hazardous Heavy Metal Waste Ash and Glass Powder," *Materials Science Forum*, vol. 1048, pp. 345-358, 2022. [CrossRef] [Google Scholar] [Publisher Link]

[25] Hemn Qader Ahmed, Dilshad Kakasor Jaf, and Sinan Abdulkhaleq Yaseen, "Comparison of the Flexural Performance and Behaviour of Fly-Ash-Based Geopolymer Concrete Beams Reinforced with CFRP and GFRP Bars," *Advances in Materials Science and Engineering*, vol. 2020, pp. 1-15, 2020. [CrossRef] [Google Scholar] [Publisher Link]

[26] Veerappan Sathish Kumar et al., "Flexural Behaviour of Hybrid Fibre-Reinforced Ternary Blend Geopolymer Concrete Beams," *Sustainability*, vol. 14, no. 10, pp. 1-16, 2022. [CrossRef] [Google Scholar] [Publisher Link]

[27] Mohamed E. Fathi et al., "Experimental and Numerical Investigation of Flexural Behavior of Sustainable Self-Compacting Geopolymer RC Beams," *Innovative Infrastructure Solutions*, vol. 11, pp. 1-18, 2025. [CrossRef] [Google Scholar] [Publisher Link]

[28] P. Saranya, Praveen Nagarajan, and Shashikala Aikot Pallikkara, "Experimental and Numerical Studies on Geopolymer Concrete Beams Under Cyclic Loading," *Practice Periodical on Structural Design and Construction*, vol. 27, no. 1, 2022. [CrossRef] [Google Scholar] [Publisher Link]

[29] Jie Su et al., "Flexural Behavior of Alkali-Activated Ultra-High-Performance Geopolymer Concrete Beams," *Buildings*, vol. 14, no. 3, pp. 1-18, 2024. [CrossRef] [Google Scholar] [Publisher Link]

[30] Deyu Zheng et al., "Flexural Performance of Composite Beams with Engineered Geopolymer Composites and Concrete: Experimental and Finite Element Analysis," *Journal of Building Engineering*, vol. 117, pp. 1-26, 2025. [CrossRef] [Google Scholar] [Publisher Link]

[31] Kafi Matloob kafi, and Ali Sabah Al Amli, "The Impact of Shear Connector Numbers on the Flexural Performance of Composite Geopolymer Reinforced Concrete Beams with Big Transverse Web Openings," *Al-Rafidain Journal of Engineering Sciences*, vol. 2, no. 1, pp. 225-238, 2024. [CrossRef] [Google Scholar] [Publisher Link]

[32] Muthusamy Saradha et al., "Flexural Behavior of Reinforced Geo-Polymer Concrete Beams at Ambient Temperature," *Pollack Periodica*, vol. 18, no. 3, pp. 8-13, 2023. [CrossRef] [Google Scholar] [Publisher Link].

[33] *ASTM C618-22 Standard Specification for Coal Fly Ash and Raw or Calcined Natural Pozzolan for Use in Concrete*, ASTM International, pp. 1-5, 2022. [CrossRef] [Google Scholar] [Publisher Link]

[34] ASTM C989/C989M-22, *Standard Specification for Slag Cement for Use in Concrete and Mortars*, American Society for Testing and Materials, pp. 1-7, 2022. [CrossRef] [Publisher Link]

[35] *ASTM C1240-20 Standard Specification for Silica Fume Used in Cementitious Mixtures*, American Society for Testing and Materials, pp. 1-7, 2020. [CrossRef] [Publisher Link]

[36] "*IS 383-2016 Coarse and Fine Aggregates from Natural Sources for Concrete*," Bureau of Indian Standards, 3rd Revision, pp. 1-22, 2016. [Publisher Link]

[37] John L. Provis, and Jannie S.J. van Deventer, *Geopolymers: Structures, Processing, Properties and Industrial Applications*, Woodhead Publishing, pp. 1-7, 2009. [Google Scholar] [Publisher Link]

[38] Samaneh Khaksefidi, Mansour Ghalehnovi, and Hosseinali Rahdar, "Bond-Slip Relationship between Deformed Rebar and Ultra-High-Performance Concrete with Corrosion Effect," *Case Studies in Construction Materials*, vol. 21, pp. 1-22, 2024. [CrossRef] [Google Scholar] [Publisher Link]

[39] Smith Songpiriyakij et al., "Anchorage of Steel Bars in Concrete by Geopolymer Paste," *Materials & Design*, vol. 32, no. 5, pp. 3021-3028, 2011. [CrossRef] [Google Scholar] [Publisher Link]

[40] Aaron Kadima Lukanu Lwa Nzambi, "Pull-out Tests of Ribbed Steel Reinforcing Bars Embedded in Concrete with Steel Fibres," *Proceedings of the Institution of Civil Engineers-Structures and Buildings*, vol. 174, no. 3, pp. 181-189, 2021. [CrossRef] [Google Scholar] [Publisher Link]

[41] "*IS 2770-1 (1967): Methods of Testing Bond in Reinforced Concrete*," Bureau of Indian Standards, pp. 1-15, 1967. [Google Scholar] [Publisher Link]

[42] "*IS 456 (2000): Plain and Reinforced Concrete - Code of Practice*," Bureau of Indian Standards, pp. 1-114, 2000. [Google Scholar] [Publisher Link]

[43] Haroon Younas, Jing Yu, and Christopher K.Y. Leung, "Effect of Bar Diameter and Cover Thickness on Bond Behavior of Steel Bar in High-Strength SHCC Under Pull-Out Condition: Experimental Study and Efficient Finite Element Modeling," *Journal of Building Engineering*, vol. 105, pp. 1-17, 2025. [CrossRef] [Google Scholar] [Publisher Link]

[44] Bilal S. Hamad, "Bond Strength Improvement of Reinforcing bars with Specially Designed Rib Geometries," *ACI Structural Journal*, vol. 92, no. 1, pp. 3-13, 1995. [CrossRef] [Google Scholar] [Publisher Link]

[45] Amr Ashraf Soliman et al., "Effects of the Tensile Properties of UHPC on the Bond Behavior," *Construction and Building Materials*, vol. 392, 2023. [CrossRef] [Google Scholar] [Publisher Link]

[46] Kui Chen, Linhao Zhang, and Xianqiao Wang, "Study on Bond Anchorage Behavior of Small-Diameter Rebar Planting under Medium and Low Cycle Fatigue Loads," *Applied Sciences*, vol. 13, no. 13, pp. 1-20, 2023. [CrossRef] [Google Scholar] [Publisher Link]

[47] "*BS 8110-1: 1997 Structural use of Concrete - Part 1: Code of Practice for Design and Construction*," British Standard, pp. 1-160, 1997. [Publisher Link]

[48] Shuaib H. Ahmad, and Roy Barker, "Flexural Behavior of Reinforced High-Strength Lightweight Concrete Beams," *Structural Journal*, vol. 88, no. 1, pp. 69-77, 1991. [CrossRef] [Google Scholar] [Publisher Link]

[49] Samir A. Ashour, "Effect of Compressive Strength and Tensile Reinforcement Ratio on Flexural Behavior of High-Strength Concrete Beams," *Engineering Structures*, vol. 22, no. 5, pp. 413-423, 2000. [CrossRef] [Google Scholar] [Publisher Link]

[50] K. Gunasekaran, R. Annadurai, and P.S. Kumar, "Study on Reinforced Lightweight Coconut Shell Concrete Beam Behavior under Flexure," *Materials & Design (1980-2015)*, vol. 46, pp. 157-167, 2013. [CrossRef] [Google Scholar] [Publisher Link]

[51] Tai-Kuang Lee, and Austin D.E. Pan, "Estimating the Relationship between Tension Reinforcement and Ductility of Reinforced Concrete Beam Sections," *Engineering Structures*, vol. 25, no. 8, pp. 1057-1067, 2003. [CrossRef] [Google Scholar] [Publisher Link]

[52] M. A. Rashid, and M. A. Mansur, "Reinforced High-Strength Concrete Beams in Flexure," *ACI Structural Journal*, vol. 102, no. 3, pp. 462-471, 2005. [CrossRef] [Google Scholar] [Publisher Link]

[53] R.N. Swamy, and G.H. Lambert, "Flexural behaviour of Reinforced Concrete Beams Made with Fly Ash Coarse Aggregates," *International Journal of Cement Composites and Lightweight Concrete*, vol. 6, no. 3, pp. 189-200, 1984. [CrossRef] [Google Scholar] [Publisher Link]

[54] M. Sivasakthi et al., "Thermal and Structural Micro Analysis of Micro Silica Blended Fly Ash based Geopolymer Composites," *Journal of Non-Crystalline Solids*, vol. 499, pp. 117-130, 2018. [CrossRef] [Google Scholar] [Publisher Link]

[55] S. Nagajothi, and S. Elavenil, "Effect of GGBS Addition on Reactivity and Microstructure Properties of Ambient Cured Fly Ash Based Geopolymer Concrete," *Silicon*, vol. 13, no. 2, pp. 507-516, 2021. [CrossRef] [Google Scholar] [Publisher Link]